Chapter

Seismic Response Characteristics of RCC Dams Considering Fluid-Structure Interaction of Dam-Reservoir System

Khaled Ghaedi, Farzad Hejazi, Meisam Gordan, Ahad Javanmardi, Hamed Khatibi and Ali Joharchi

Abstract

In analysis of different types of dams, i.e. arch, gravity, rockfill and Roller Compacted Concrete (RCC) dams, the effect of hydrodynamic water pressure as an effective factor must seriously be taken into consideration. In present study, the hydrodynamic effect is precisely deliberated in RCC dams and compared to hydrostatic pressure effect. For this purpose, Kinta RCC dam in Malaysia is selected and 2D finite element (FE) model of the dam is performed. The Lagrangian approach is used to solve the dam-reservoir interaction, fluid–structure interaction (FSI), and in order to evaluate the crack pattern, Concrete Damaged Plasticity (CDP) model is implemented. Comparisons show that hydrodynamic pressure significantly changes the dam behaviour under seismic excitations. Moreover, the hydrodynamic effect modifies the deformation shape of the dam during the ground motions, however, it increases the magnitudes of the developed stresses causing more extensive tension crack damages mostly in the heel and upstream zones of the dam.

Keywords: fluid–structure interaction, hydrodynamic pressure, earthquake, concrete damaged plasticity, Kinta dam

1. Introduction

Earthquake as an unpredictable event [1] is one of the main concerns of structural engineers. However, to protect civil structures such as buildings and bridges against ground motions several approaches have so far been used [2–9], but more attention must be payed to construct water control structures such as dams, where the water weight effect combined with earthquake force increases the danger of structural destruction. Recently, application of RCC technology in dam construction was launched, early 2002. This technology provides some advantages for dam engineers in terms of equipment, manpower, construction speed and cost. Analysis of gravity dams subjected to earthquake excitations considering different aspects of analysis including interactions, boundary conditions, reservoir length and height have been addressed by many researchers [10–15]. The difference between constitutive relationship of RCC and conventional concrete invites the investigators to study different aspects of analysis of the RCC dams such as dam-foundation,

dam-reservoir and dam-reservoir-foundation interaction. For instance, Fenves and Chopra [16] presented a simplified method to evaluate the response of concrete gravity dams utilizing fundamental vibration mode considering dam-reservoir with impounded water interaction and dam-foundation interaction. Malkar [17] investigated the seismic responses of several gravity dams considering different heights by means of Automatic Dynamic Incremental Nonlinear Analysis (ADINA) code. The crack propagation model was also investigated using fracture criterion of tensile stresses. Ayari [18] used the effective simulation of fracture mechanics and discrete crack (DC) closure under transient dynamic circumstances to develop new models in order to investigate the crack propagation of concrete gravity dams. To this end, the Koyna gravity dam was selected to be analysed. Espandar and Lotfi [19] applied bidirectional accelerations to the Shahid Rajaee arch dam to investigate the nonlinear seismic response of the dam using the nonlinear techniques of continuum mechanics i.e. elasto-plastic and non-orthogonal smeared crack (NOSC) models. Later on, the accuracy of the models was compared to experimental results. It was concluded that, the NOSC model was much better than the linear elastic analysis to evaluate the dam stresses. Lotfi and Espandar [20] developed a special FE program using combination of DC and NOSC methods, known as DC-NOSC technique, which was employed to examine the nonlinear behaviour of an arc dam. It was found that the results of the DC-NOSC model were more reliable compared to DC and NOSC method used alone. Akkose et al. [21] examined the response of arc dams considering the effect of different water levels. The yield criterion of Drucker–Prager was implemented to idealize the concrete dam in nonlinear analysis. The reservoir water was modelled according to the Lagrangian method. Akkose and Simsek [22] investigated the influence of both near- and far-fault excitations on the nonlinear response of a gravity dam considering dam-reservoir-foundation-sediment interaction. Kartal [23] imposed a three-directional earthquake to a RCC dam in order to study the response of the dam considering material and geometry. The effect of reservoir water was inspected using the Lagrangian method through fluid FEM. Zhang et al. [24] investigated the effect of strong after-shocks and their potential to damage the concrete gravity dams. Hence, the hardening behaviour was taken into account for material properties of the dams to deliberate the crack propagation. Ghaedi et al. [25] studied the influence of flexible foundations on seismic response of RCC dams using FEM considering hydrodynamic pressure of the reservoir water. Wang et al. [26] studied the correlation between period of ground excitations and damage severity in gravity dams using twenty ground motion records with different time frames. They showed that, durations of the ground motions had no remarkable effect on damage levels. Ghaedi et al. [27] investigated the effect of openings (galleries) considering different sizes and shapes on dynamic response of RCC dams. The results showed that, RCC dams with circular openings behave better compared to other geometric shapes such assquare and octagon. Wang and Jia [28] made an attempt to propose a new approach to test and design hydraulic fracturing of high concrete gravity dams with more than 200 m height. For that purpose, a cylindrical sample with embedded crack was prepared to model the hydraulic fracture of concrete gravity dam heel, while the sample was subjected to a uniaxial load at both ends of the sample. Wang et al. [29] constructed a large-scale concrete-rockfill combination dam (CRCD) and crucial factors such as deformation, acceleration time history, slope failure and dynamic earth pressure were examined to investigate the dynamic performance of the CRCD.

Based on the above literature, it is a crucial issue to take hydrodynamic reservoir pressure effect into account in order to investigate the behaviour of RCC dams under seismic motions. To aid the aim, an attempt is made to investigate the

nonlinear behaviour of a RCC dam subjected to earthquake excitations considering the hydrodynamic water pressure effect through the Lagrangian approach. For this purpose, Kinta RCC dam located in Malaysia is chosen as a case study and a two-dimensional Finite Element Model (FEM) is implemented via ABAQUS software. In order to predict the crack propagation, the Concrete Damaged Plasticity (CDP) model is used. In addition, the model change technique is used to model the RCC layers of the dam.

2. Kinta RCC dam (case study)

The Kinta RCC dam location in the city of Ipoh, 205 km north from Kuala Lumpur. The Kinta dam is the first constructed RCC dam in Malaysia, as shown in **Figure 1**, and for the first time RCC technology had been utilized in the world to construct the steps of spillway. To build the dam, RCC with zero-slump was used while several slim horizontal layers were compacted using vibratory rollers. In the present study, the Kinta RCC dam is chosen as a case study to evaluate the seismic behaviour of the dam when the effect of reservoir water pressure is taken into consideration. The structural geometry of the deepest section of the Kinta RCC dam used in the study is depicted in **Figure 2** [31] (see also [27]).

As shown in **Figure 2**, the dam comprises three sections including the dam body which is surrounded by Conventional Vibrated Concrete (CVC) upstream and downstream face as well as CVC foundation.

3. Finite element model (FEM)

For eismic analysis of the Kinta RCC dam, the dam is accurately modelled using FE software, ABAQUS. To discretize the dam body as well as CVCs, a 2D isoparametric elements with four nodes bilinear plane stress quadrilateral, reduced integration and hourglass control is implemented. Besides, to discrete the reservoir

Figure 1.
Location of Kinta RCC dam.

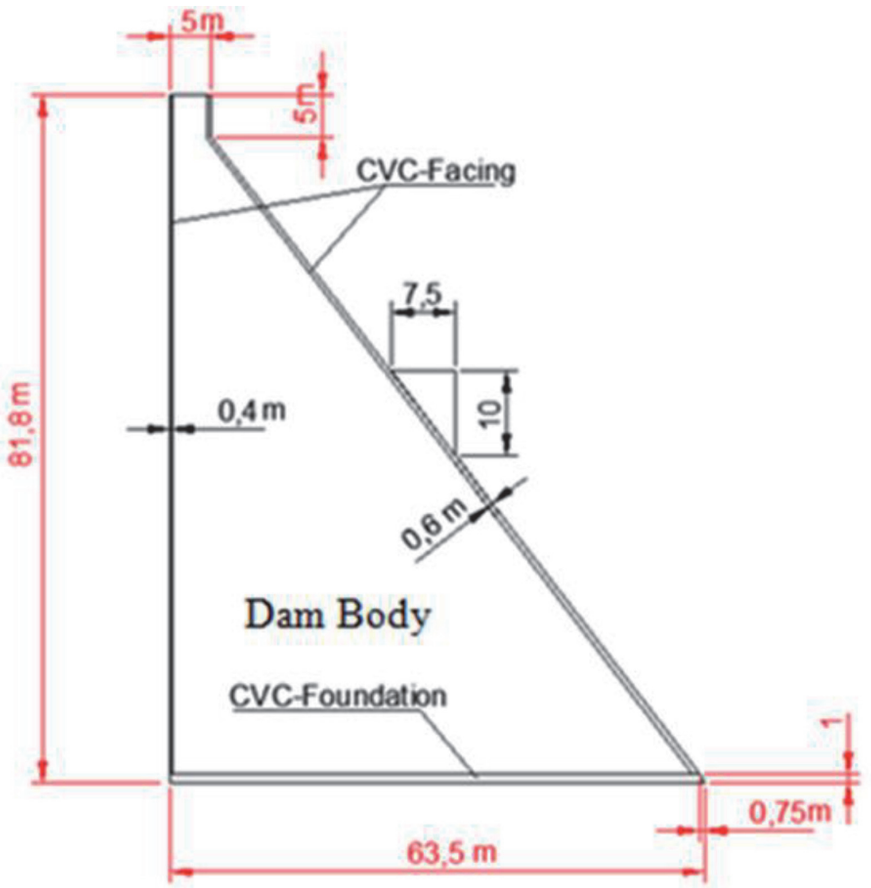

Figure 2.
Geometry of the Kinta RCC dam [30].

Block	No. of nodes	No. of elements
Dam Body	609	560
CVC Upstream Facing	56	27
CVC Downstream Facing	58	26
CVC Foundation	42	19
Reservoir Water	551	504

Table 1.
Finite element discretization of the Kinta RCC dam.

water, a 2D acoustic quadrilateral FE with four nodes linear is conducted. The details of the dam and CVCs discretization are indicated in **Table 1**. **Figure 3** shows the FEM of the Kinta dam. Furthermore, the material properties are used for modelling of the dam as demonstrated in **Table 2** [32]. The tensile strength is characterized as 10% of the compressive strength [33]. The density, ρ, and the bulk modulus, K_w, for the reservoir water are taken as 1000 Kg/m^3 and 2107 MPa, respectively.

3.1 Fluid–structure interaction (FSI)

Three basic methods are frequently utilized to solve the fluid–structure interactions using the FEM, i.e. Eulerian method, Westergaard method, and Lagrangian method. In Eulerian method, translations (displacements) are considered as variables in structure, whereas, variables of fluid are pressures. Because the structure and

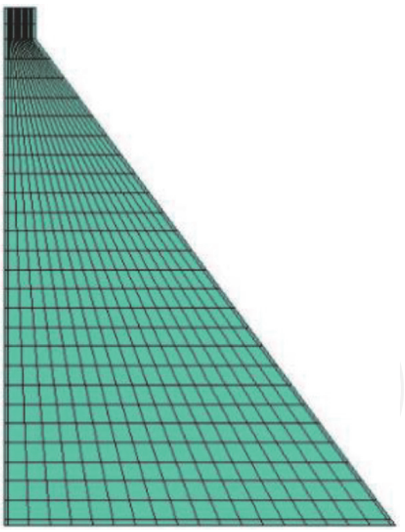

Figure 3.
FEM of the Kinta RCC dam.

Material property	Young modulus (MPa)	Poisson ratio	Density (Kg/m^3)	$\sigma_{cu}\sigma_{cu}$ (MPa) Ultimate compressive stress	σ_{tu} (MPa) Ultimate tensile stress
RCC DAM BODY	23000	0.2	2386	20	2.5
CVC-FACING	32000	0.2	2352	40	5
CVC-FOUNDATION	23000	0.2	2325	20	2.5

Table 2.
Material properties used in the present study.

fluid variables are not same in this method, a special purpose computer is required to solve the coupled systems. In Westergaard method, added mass, connected to the structure, is used to represent fluid–structure system. In Lagrangian method, variables in both fluid and structure are similar. Therefore, in this method the equilibrium as well as the compatibilities are repeatedly converged along the interface nodes. This is displacement-based FE for fluid elements that is quite appropriate because it is not required unusual interface equations and it can be performed via general-purpose computers [27]. As a result, in the present study in order to investigate the effect of water pressure, the Lagrangian method was used.

3.2 Finite element equation

The FSI has to be considered for purpose of the nonlinear analysis of the dam during earthquake excitation. Therefore, the finite element discretization of the differential equation defines the displacement of the dam structure as below:

$$M_s\ddot{u} + C_s\dot{u} + K_s = F_g + F_P \tag{1}$$

where the M_s is mass and C_s and K_s are damping and stiffness, respectively. $\ddot{u}, \dot{u}$ and $u\acute{u}, \acute{u}\wedge u$ are the relative acceleration, velocity and displacement of the dam with respect to the time, t. In addition, F_g and F_P are the force and extra force vectors described as:

$$F_g = -M_s I\ddot{u}_g(t) \tag{2}$$

and

$$F_P = \mathrm{QP} \tag{3}$$

In which, I is the influence vector and F_P is the hydrodynamic force acting towards the dam at the upstream face. This force is a function of unidentified parameters of the nodal pressure vector of the water, P, through the transformation matrix, Q, that is determined as:

$$Q = \int N_U^T n N_p \mathrm{dr} \tag{4}$$

where N_p is the shape function of the pressure fields and N_U is the nodal displacement of the dam. r_1 is the dam-reservoir interface and n is the unit normal vector. This explanation is owing to the discretization of the boundary conditions. The energy dissipation inside the dam is also categorized by the Rayleigh damping matrix that is written as below equation:

$$C_s = \alpha M_s + \beta K_s \tag{5}$$

in which α and β are the Rayleigh damping parameters of the first and last mode of vibrations. It is commonly agreed that, damping ratios of the dams have a range between approximately 2–5%. For all mode of vibrations, herein, the properties of material damping are adjusted to be as 5% fraction of the critical damping [27] for the first mode of the dam vibration during the dynamic analysis. In the present study, the damping ratio (5%) is tuned for the entire dam under free vibration. Accordance with this analysis, the natural frequencies of the dam are determined and ranged between ω_1= 9.571 Hz and ω_2= 51.238 Hz for the first and last mode of the dam vibrations. Consequently, by taking the natural frequencies into consideration, the values of the Rayleigh damping parameters are obtained as α = 0.806 and β = 0.00164 in the dynamic analysis of the Kinta RCC dam [34] in this study.

3.3 Coupled dam-reservoir (FSI) equations

During earthquake motions, the dam interacts with reservoir. Thus, the hydrodynamic pressure effect owing to the reservoir water and its interaction with the dam has to be taken into account. Consequently, to deliberate the reservoir hydrodynamic pressure, the force vector, F_q, due to the acceleration ($\ddot{u}$) is imposed to the upstream side of the dam. Accordingly, the force vector can be determined as:

$$F_q = -\int_{r_1} N_p^T \rho \ddot{u}.\mathrm{ndr} \tag{6}$$

Substituting the acceleration vector into the nodal vector, that is $\ddot{u} = N_u \ddot{U}$ provides the transposed matrix of the Q^T in Eq. (4). Multiplying the transposed matrix by reservoir water density, ρ, presents the equation below:

$$K_F P = -\rho Q^T \ddot{U} \tag{7}$$

In which, $K_F = \left[G^{-1}\right]^T [A] \left[G^{-1}\right]$, A is the linear element matrix, G is the basic solution of Laplace's equation or Green function and $K_F P = F_q$. Then, the pressure vector can be concluded as:

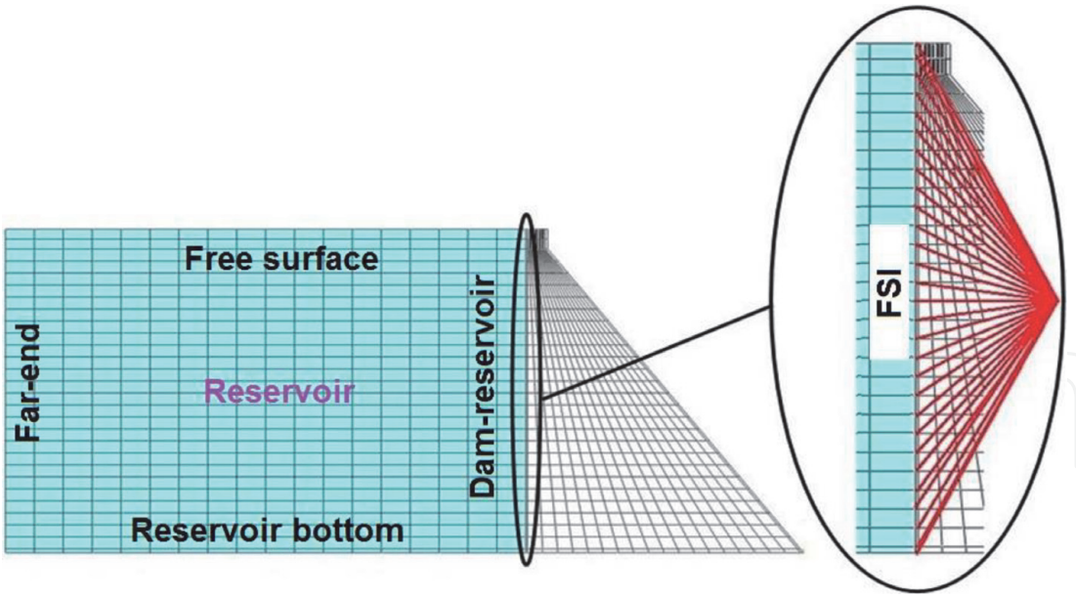

Figure 4.
Boundary conditions of the Kinta dam-reservoir system.

$$P = -\rho K_F^{-1} Q^T \ddot{U} \tag{8}$$

Substituting Eq. (8) into Eq. (3) gives the dynamic equation for displacement of the structure as below:

$$\left[M_s + \rho \mathrm{Q} \mathrm{K}_F^{-1} Q^T\right] \ddot{U} + C_s \ddot{U} + K_s U = \mathrm{F} \tag{9}$$

This is the renowned equation in FEM for solving fluid–structure systems. In this study, the reservoir water pressure is subjected to the boundary conditions at: (1) reservoir bottom (2) free surface of the reservoir (3) reservoir far-end and (4) upstream side of the dam as described by [27] and as depicted in **Figure 4**. For FSI, node to node interaction method is used in order to assess the real behaviour of the RCC dam during seismic excitation.

4. Concrete damaged plasticity (CDP)

The linear assumption may not be fit to investigate RCC dams subjected to dynamic motions [35–38]. To date, many techniques such as smeared crack model, isotropic and anisotropic damage model have proposed to investigate the constitutive model of concrete materials and their complex mechanical reaction while subjected to ground excitations. In this regard, a basic model known as plastic-damage model was proposed [39] and adapted [40]. The nonlinear performance of each synthetic material in a multiphase compounded material is commonly expressed by the CDP model and it can be used to examine the cracking. Besides, the CDP model factorizes the uniaxial compressive and tensile strength into two parts to describe the permanent degradation of stiffness and deformation. The plastic-damage model considers two major failure mechanisms for concrete materials in both compression and tension conditions, namely crushing and cracking, respectively.

The incremental theory of plasticity splits the strain tensor (ε) into two sections, i.e. the elastic strain (ε^e) and the plastic strain (ε^p) in which the equation of linear elasticity can be written as:

$$\varepsilon = \varepsilon^e + \varepsilon^p \tag{10}$$

The variables $\{\varepsilon^e, \varepsilon^p, \kappa\}$ are time-dependent. By using these parameters, the below equation can express the stress tensor:

$$\sigma = (1-d)\bar{\sigma} = (1-d)E_0(\varepsilon - \varepsilon^p) \tag{11}$$

Where $d = d(\kappa)$ is the scalar stiffness degradation which ranges from 0 (undamaged) to 1 (fully damaged); E_0 is the undamaged elastic stiffness. The material failure mechanism associates with damage, thus, reduction of the elastic stiffness is considered as a function of the internal variable (κ) i.e. compressive and tensile variables; $\kappa = (\kappa_c, \kappa_t)$. The damage functions, tension (d_t) and compression (d_c), are considered as the nonlinear functions and they can be calculated using uniaxial compressive response alongside with practical data. Therefore, the effective stress can be defined as:

$$\bar{\sigma} = (\sigma/1-d) = E_0(\varepsilon - \varepsilon^p) \tag{12}$$

5. Loading on the dam

5.1 Hydrostatic load

Dams are usually constructed for the purpose of raising the water level of waterways on the upstream face. The rising water results hydrostatic pressure and leads the structure to slip horizontally and overturn about the toe or bottom edge of the downstream side. This pressure acts as a linear force along the dam height. In this study, the hydrostatic pressure is considered as a perpendicular force to the upstream surface so that the hydrostatic pressure is increased linearly along the dam height from zero at the free surface to 802458 Pa at the base level of the Kinta dam in the upstream side.

5.2 Hydrodynamic load

Vertical acceleration of an earthquake decreases the unit weight of material of concrete dams and the horizontal component acting on the stored water results an immediate pressure increase in the reservoir water. As a result, dam accelerates in direction of the reservoir when the water attempts to prevent the motion because of its inertia. The further pressure applied with this trend is called hydrodynamic pressure. In the present study, a reservoir with a height of 81.8 m, as displayed in **Figure 5**, is modelled to validate the hydrodynamic force at the interface of the dam-reservoir. An attempt is made to consider the hydrodynamic pressure by modeling of the accumulated water at the upstream face of the dam body. The foundation is assumed to be rigid and the impounded water in the reservoir is considered as the compressible fluid during the analysis, while the sediment absorption effect of the reservoir bottom is not deliberated.

5.3 Seismic Loading

To investigate the effect of earthquake motions on the Kinta RCC dam, Koyna earthquake records (India, 1967) with peak ground acceleration (PGA) of 0.47 g in horizontal (longitudinal) direction and 0.31 g in vertical (transverse) direction were

Figure 5.
Dam-reservoir model used to study hydrodynamic pressure on the Kinta RCC dam.

applied to the Kinta dam, as shown in **Figure 6**. The period of the applied earthquake is selected for 10 seconds with defining step time of 0.01 second for each interval during excitations.

6. Results and discussions

Prior to the interpretation of results and discussions, it is necessary to define the topmost node and the lowest node of the modelled dam at the upstream face in order to investigate the maximum relative acceleration and displacement response of the dam. In other words, to obtain the maximum relative acceleration and displacement response, the difference of the maximum acceleration and displacement responses of the topmost node and the lowest node (nodal acceleration and nodal displacement) has to be taken into account. For this purpose, the nodes located at the dam crest and heel zone is selected as shown in **Figure 7**.

6.1 Displacement response

The relative horizontal and vertical displacements of different dams have been reported by many researchers. Herein, the maximum relative horizontal displacement of the dam crest with hydrostatic and hydrodynamic pressure effect is investigated and indicated in **Figure 8**. As it is obvious in the figure, the seismic response of the relative horizontal displacement of the dam crest is 2.32 cm at 4.02 second due to the hydrostatic pressure and 2.8 cm at 3.689 second due to the hydrodynamic water pressure. The occurred horizontal displacements for both cases at the mentioned seconds are also demonstrated in **Figures 10(a)** and **11(a)** as the displacement contour. Therefore by subtracting the values in those figures, the relative

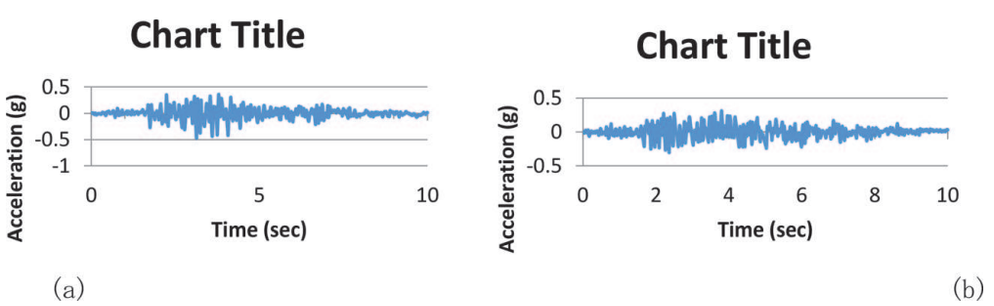

Figure 6.
(a) Horizontal and (b) Vertical acceleration of the Koyna excitations (India, 1967).

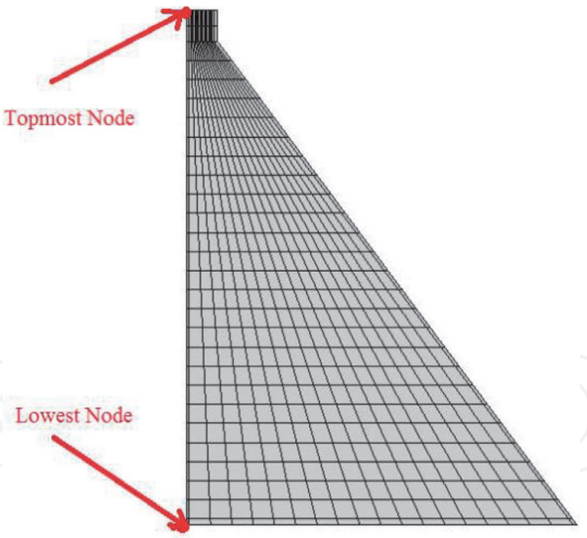

Figure 7.
The location of the topmost node (crest) and the lowest node (heel) at the upstream face.

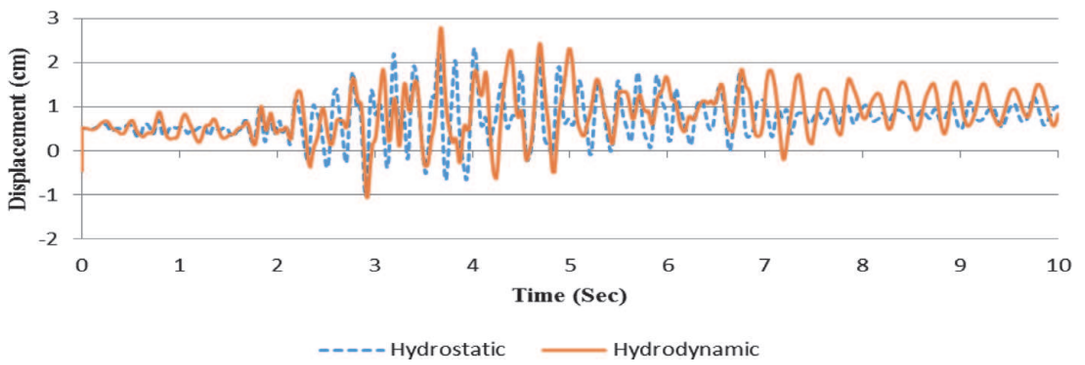

Figure 8.
Relative horizontal displacement of the dam.

displacement can be obtained. For instance in **Figure 10(a)**, 17.30 cm – 14.98 cm = 2.32 cm. This values confirm that the displacement response is increased by 21% when the influence of the hydrodynamic pressure is taken into consideration. In addition to this, the movement is in the positive direction towards the downstream side.

In like manner, the maximum relative vertical displacement of the Kinta dam is shown in **Figure 9**. Based on this figure, the relative vertical displacement of the dam is −0.7 cm at 4.024 second for the hydrostatic effect and − 1.17 cm at 4.391 second for the hydrodynamic water effect. This effect is also shown in **Figures 10(b)** and **11(b)** which are selected at the mentioned seconds. This difference in values again proves the significant effect of hydrodynamic pressure by 67% increase in the vertical direction.

The displacement contours of the Kinta RCC dam in the horizontal and vertical directions due to the Koyna earthquake considering the hydrostatic and hydrodynamic pressure effect are shown in **Figures 10** and **11**. The selected seconds in these figures is chosen accordance with **Figures 8** and **9** in which the maximum relative horizontal and vertical displacement of the RCC dam is occurred. As depicted in **Figure 10(a)**, the nodal horizontal displacement of the dam crest and the heel is 17.30 cm and 14.98 cm, respectively when the hydrostatic pressure is taken into account (17.30–14.98 = 2.32 cm which was described in **Figure 8** as the relative horizontal displacement), whereas, the nodal horizontal displacement of the crest

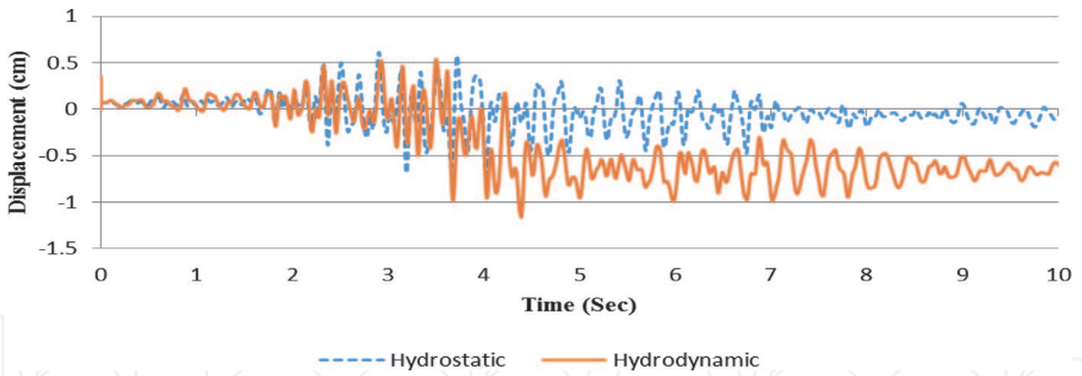

Figure 9.
Relative vertical displacement of the dam.

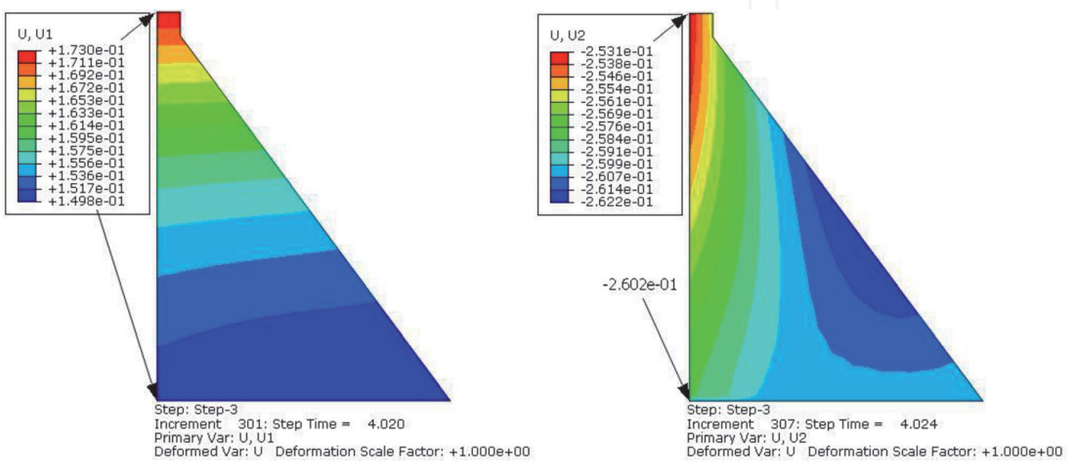

Figure 10.
Displacement (m) contours considering the hydrostatic pressure. (a) Horizontal direction. (b) Vertical direction.

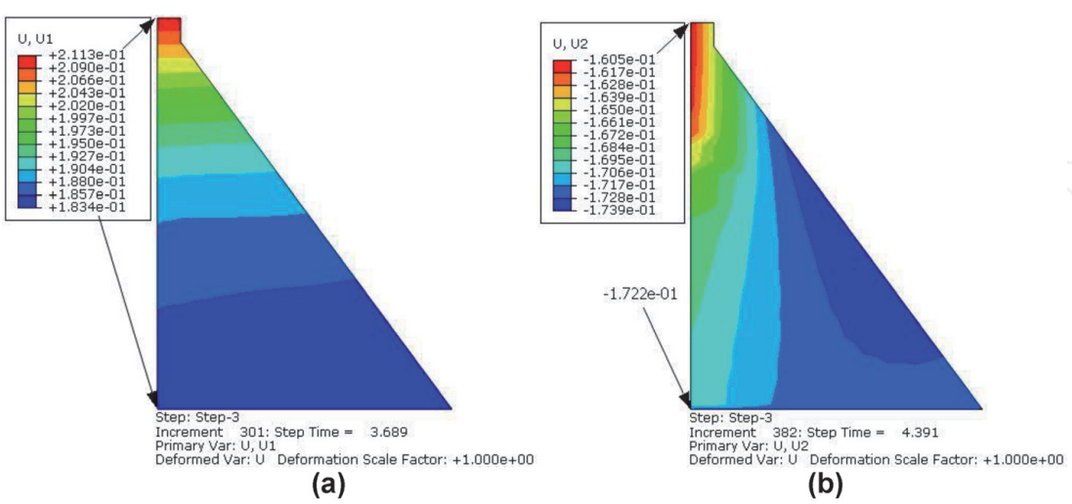

Figure 11.
Displacement (m) contours considering the hydrodynamic pressure. (a) Horizontal. (b) Vertical.

and the heel is 21.13 cm and 18.34 cm considering hydrodynamic water pressure effect (21.13–18.34 = 2.8 cm which was shown in **Figure 8** as the relative horizontal displacement). The comparison of the difference between obtained values shows the hydrodynamic water effect by 22% increase in the horizontal displacement response of the dam. On the other hand, **Figures 10(b)** and **11(b)** illustrate the

maximum vertical displacement of the crest and heel nodes of the dam. As depicted in **Figure 10(b)**, the nodal vertical displacement of the dam crest and the heel is 25.31 cm and 26.02 cm, respectively when the hydrostatic pressure is taken into account (25.31–26.02 = −0.7 cm which was described in **Figure 9** as the relative vertical displacement), whereas, the nodal vertical displacement of the crest and the heel is 16.05 cm and 17.22 cm considering hydrodynamic water pressure effect (16.05–17.22 = −1.17 cm which was shown in **Figure 9** as the relative vertical displacement). The comparison of the difference between obtained values shows the hydrodynamic water effect by approximately 36% reduction in the vertical displacement response of the dam. It is because that, the modelled water alongside its assigned weight in the hydrodynamic situation causes smaller vertical movement on both the crest and heel nodes compared to same movements of the aforesaid nodes deliberating the hydrostatic effect on the upstream side.

6.2 Acceleration response

The values of the relative horizontal and vertical acceleration of the dam are indicated in **Figures 12** and **13**. It can be seen from **Figure 12** that, the increase of acceleration response of the dam by 7% from 4 m/s^2 to 4.28 m/s^2 confirms the effect of hydrodynamic pressure on the nonlinear dynamic analysis. However, absorption of acceleration by 2.2 m/s^2 in vertical direction considering the hydrodynamic water effect is approximately similar in compare to the hydrostatic water effect which is only 2.3 m/s^2.

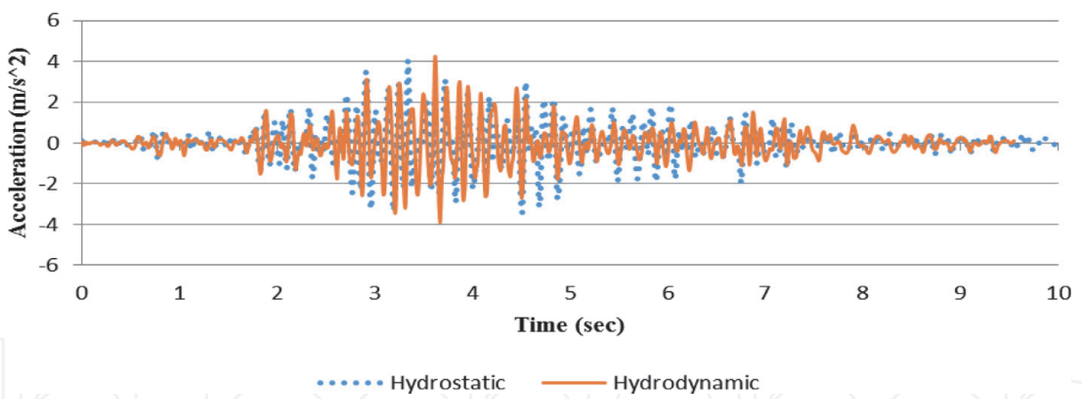

Figure 12.
Relative horizontal acceleration.

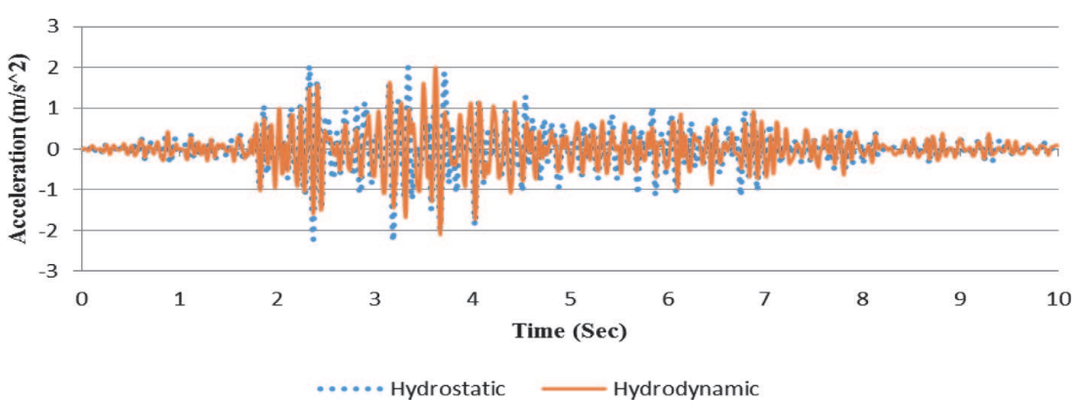

Figure 13.
Relative vertical acceleration.

6.3 Stress

Time history analysis of the maximum principal stresses at the crest and heel elements considering hydrostatic and hydrodynamic pressure effect is plotted in **Figure 14**. It can be seen from the figure that, unlike to the heel element, which experiences the maximum principal stress at initial seconds of the excitations, the crest element experiences no stress at the upstream face in both hydrostatic and hydrodynamic conditions up to second 1.81. Later on, the crest element starts to take an amount of stress and obtains its highest value by 0.195 MPa at 3.19 second under hydrostatic water effect and 0.212 MPa at 3.68 second under hydrodynamic water effect. For the heel element, as shown in **Figure 14(a)** and **(b)**, the stress value is 2.37 MPa at approximately 0.001 second from the earthquake initiation considering both hydrostatic and hydrodynamic pressure effect on the dam. Take note that, the stresses in the heel element after about 5 second is approximately zero. Since during earthquake the stress is changed from an element to another, therefore, after this period the heel element almost does not absorb any serious stress like the other elements. **Figure 15** indicates the maximum principal stresses taken by the heel element (considered as the critical element) at the exact second of absorbing the maximum stress (0.001 second) as expressed above.

Figure 16 indicates the time history analysis of the minimum principal stresses of the crest and heel elements considering hydrostatic and hydrodynamic water pressure. As indicated in the figure, for both the crest and heel elements, the stress

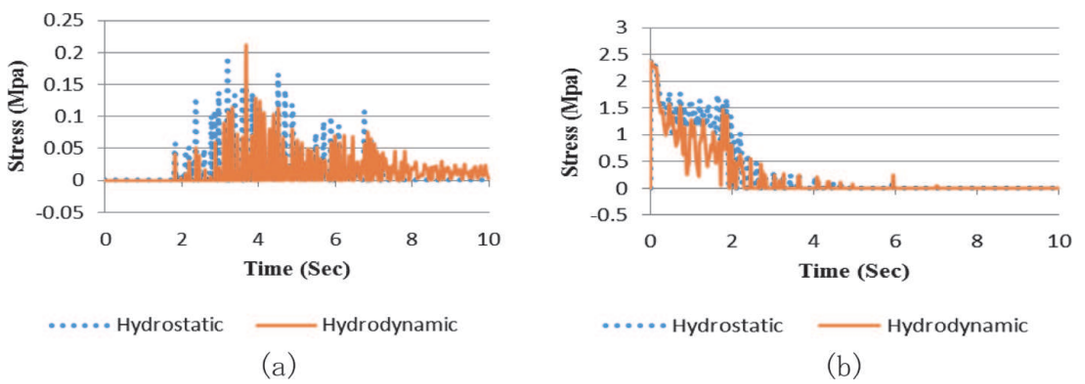

Figure 14.
Time history of the maximum principal stress at the upstream face. (a) Crest element. (b) Heel element.

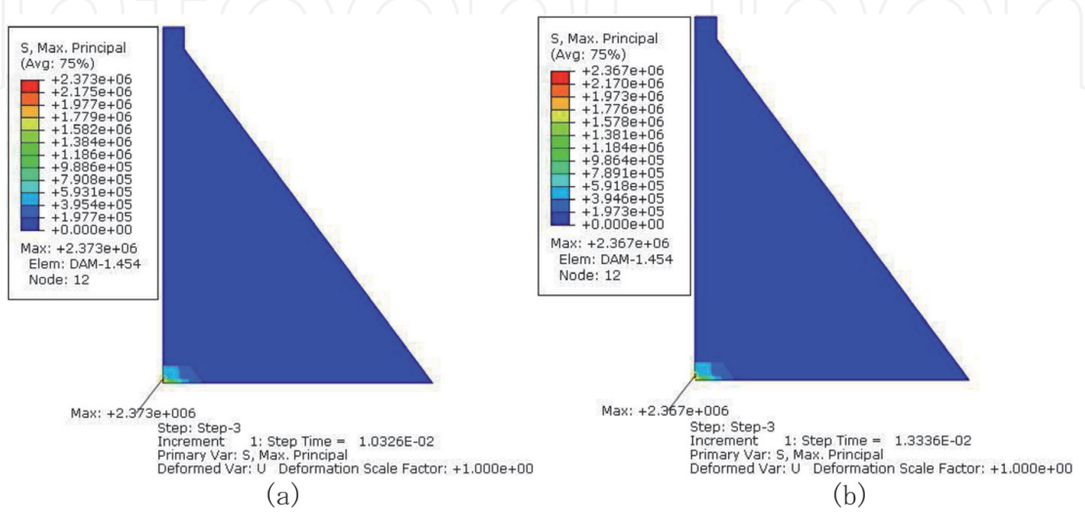

Figure 15.
Maximum principal stress contour of the Kinta RCC dam considering heel element. (a) Hydrostatic effect. (b) Hydrodynamic effect.

is smaller when the hydrodynamic water pressure is deliberated. The minimum principal stress for the crest element is −0.283 MPa considering the hydrostatic effect and − 0.256 MPa considering the hydrodynamic pressure effect as shown in **Figure 16(a)**. Moreover, the time history of the minimum principal stresses attracted by the heel element during the analysis is demonstrated in **Figure 16(b)**. The minimum stress value of the element where the dam interacts with the hydrostatic pressure is −7.84 MPa and − 6.10 MPa in the hydrodynamic interaction condition (22% reduction). **Figure 17(a)** and **(b)** displays the stress contour of the dam at the selected seconds so that the minimum stress values is occurred on the heel element, as explained in **Figure 16(b)**, in both the hydrostatic and hydrodynamic conditions. Apart from the stress values of the heel element in both conditions, the stress propagation inside the dam body is also demonstrated that, the hydrodynamic pressure can influence and change the stress pattern of the dam at different time frame of the analysis.

6.4 Seismic damage of the RCC dam

In the present study, the evaluation of damage level and assessment of the seismic performance of the dam is conducted based on the Concrete Damaged Plasticity (CDP) model. The tensile damage of the considered models is displayed in

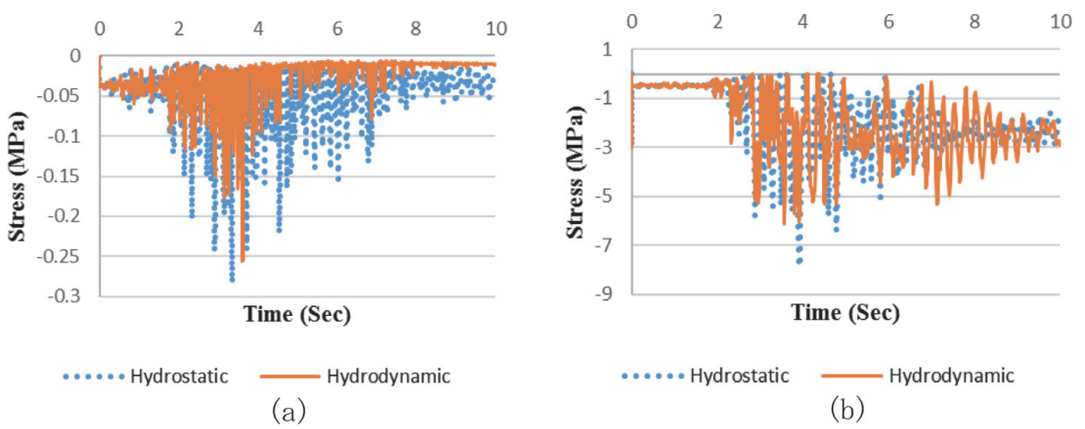

Figure 16.
Time history of the minimum principal stress at the upstream face. (a) Crest element. (b) Heel element.

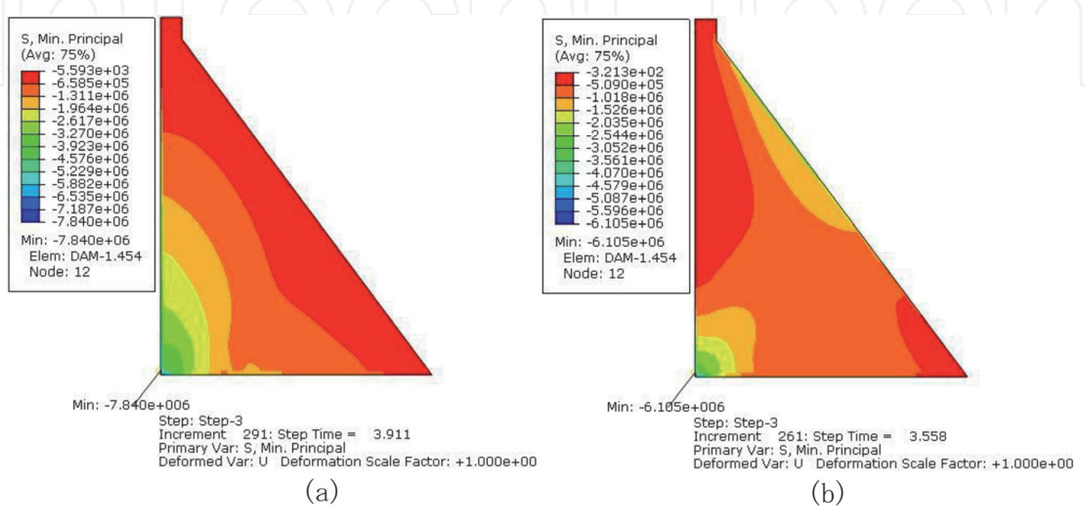

Figure 17.
Minimum principal stress contour of the Kinta RCC dam considering heel element. (a) Hydrostatic effect. (b) Hydrodynamic effect.

Figure 18. Accordance to this figure, the dam in both cases experiences damage (cracking) at the heel elements in the upstream side. Although, the onset of crack pattern is formed in the upstream side at the heel elements, but as the acceleration intensifies, the cracks propagate and develop in different zones of the dam considering the hydrodynamic water effect. **Figure 18(a)** illustrates the crack propagation for the hydrostatic condition which is started from heel zone. When the crack is initiated, it propagates in the horizontal direction toward the downstream side. **Figure 18(b)** gives a picture of tensile damage (cracking) owing to the hydrodynamic effect. As depicted in the figure, the severity of cracking of the dam due to the hydrodynamic pressure effect is not limited to the heel elements but also the dam suffered from additional cracks at the middle zone of the upstream side. This confirms the significance of the nonlinear analysis of the dam considering hydrodynamic pressure effect under seismic ground motions.

Numerous researchers have investigated and reported failure (sliding) mechanism of dams using different approaches [41–45]. It can be concluded from the literature that, there is a direct relationship between opening cracks and sliding (failure) mechanism. Thus, in this study the failure mechanism of the dam and particularly in the heel elements, as the critical elements, considering hydrodynamic pressure effect is presented in **Figure 19**. **Figure 19(a)** shows the crack propagation opf the Kinta RCC dam at the end of the seismic analysis considering hydrodynamic water pressure effect (as is previously illustrated in **Figure 18(b)**). Since, the heel elements at the upstream face are the first elements prone to cracking, therefore, it is tried to investigate the dam failure due to cracking of these elements because of overturning moment owing to the combined effect of the hydrodynamic force and ground motions as shown in **Figure 19(b)**.

According to **Figure 19(a)**, the Kinta RCC dam experiences cracking at the heel elements nearby the upstream face, whilst, the downstream face has no sign of cracking. But, due to the dam overturning and according to description of **Figure 19 (b)**, at the end of the analysis the RCC dam has a movement with magnitude of 12.57 cm (7.65 cm in horizontal direction and 9.97 cm in vertical direction), exactly at the last element of the dam toe. As shown in **Figure 19(a)**, the first six elements are fully cracked and influence the next three elements to be as semi-cracked elements, whereas other 11 elements (elements number 479–489) towards the downstream side are not cracked.

The time history of crack propagation of the heel element (as the critical element) considering hydrostatic and hydrodynamic water pressure effect under the

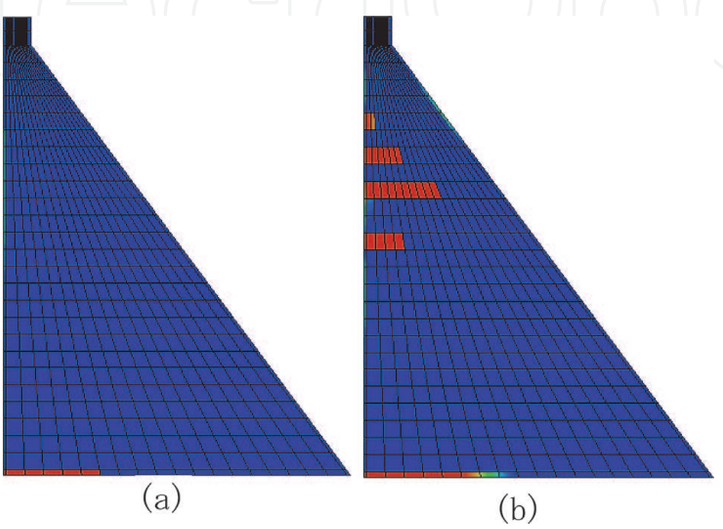

Figure 18.
Tensile damage at the end of analysis. (a) Hydrostatic effect. (b) Hydrodynamic effect.

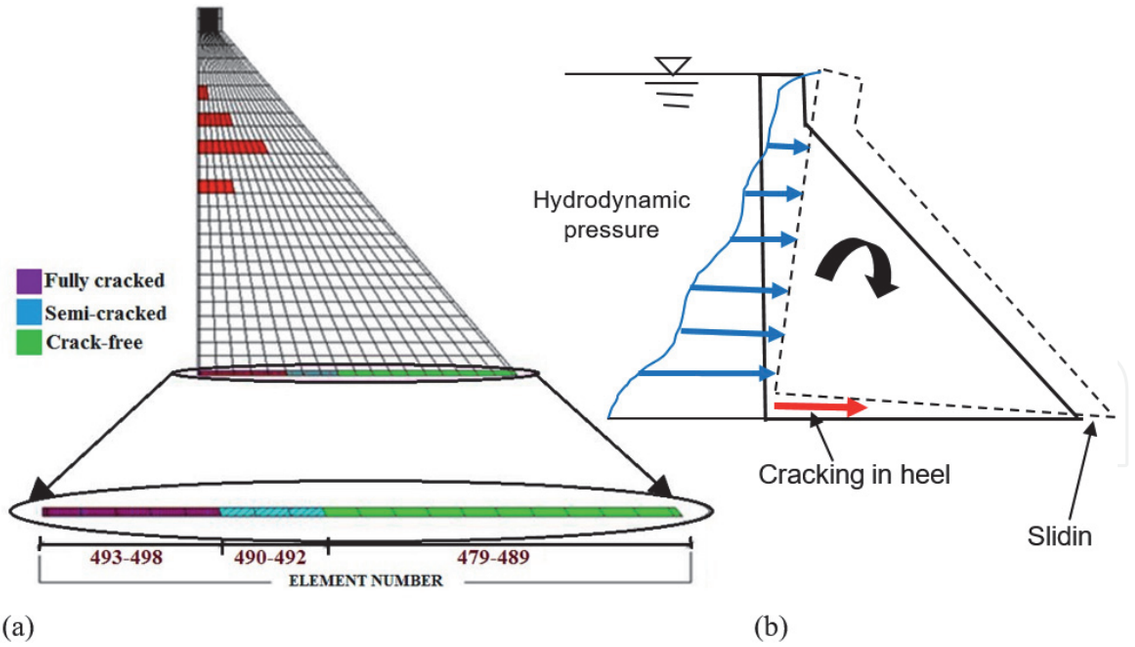

Figure 19.
Failure (sliding) mechanism of the dam during seismic excitations. (a) selected elements. (b) sliding mechanism.

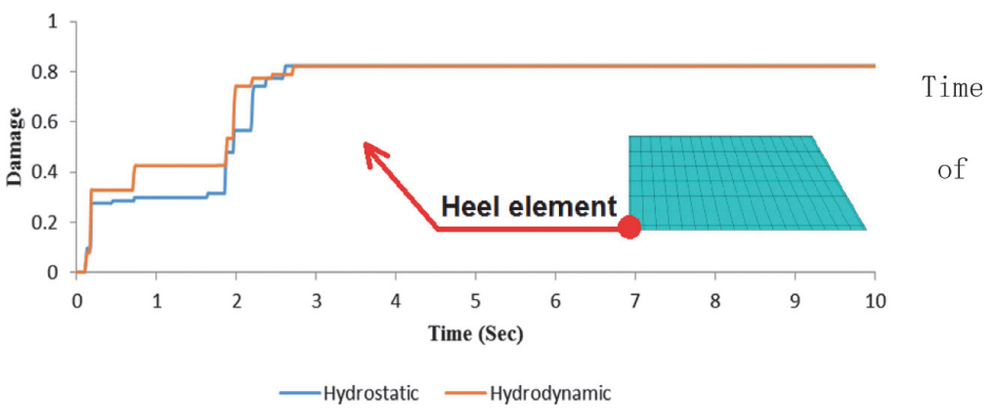

Figure 20.
Time history analysis of damage (cracking) development procedure of the selected heel element.

Koyna excitation is indicated in **Figure 20**. The damage range in this figure is provided based on the concrete tension stiffening used in the modeled dam which has direct relation to the tensile strength of the dam concrete as presented in **Table 2**. Based on this explanation and from **Figure 20** it can be concluded that, the heel element until 0.137 second under both hydrostatic and hydrodynamic water pressure effect does not take any damage (cracking). Increasing the reservoir water pressure effect, especially in the hydrodynamic condition, expedites the damage (cracking) procedure of the heel element and leads the dam to experience cracking in the heel zone faster than the condition that the hydrostatic effect is present. Consequently, it is an important matter for the nonlinear seismic analysis of dams to take the hydrodynamic water pressure effect into consideration.

Figure 21 displays the tensile damage process for both the hydrostatic and hydrodynamic conditions during the nonlinear analysis. As given in this figure, some selected times are taken to show the development of cracking inside the dam body under seismic loading. It can be detected from the figure that, from initial time up to 2.73 second the crack propagation trends same pattern. By increasing the

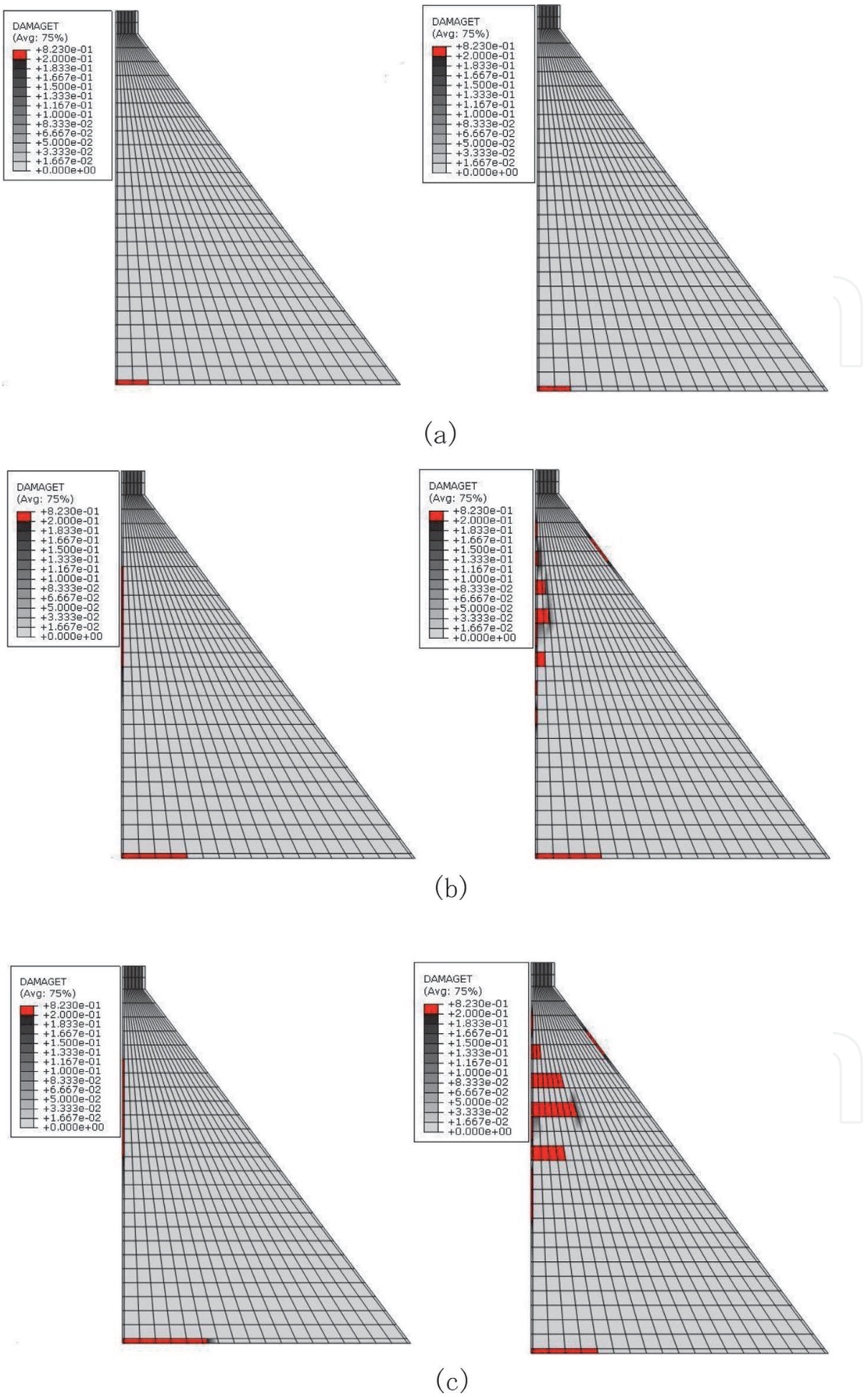

Figure 21.
Tensile damage (cracking) of the Kinta RCC dam at different times considering reservoir hydrostatic (left side) and hydrodynamic (right side) pressure effect. (a) Extension of crack, t = 2.73 sec. (b) Crack propagation at the base affecting more neighboring finite elements, t = 3.67 sec. (c) Severe cracking, t = 4.03 sec.

seismic load and by nearing to the PGA of the Koyna earthquake, at time 3.67 second, the cracks appear with different propagation inside the dam body. At this time it is clear that, the cracking launches at the upstream face towards the downstream direction taking the hydrodynamic pressure effect into consideration. At the time 4.03 second, the orientation of cracking is trended at same level from the heel elements to downstream direction considering the hydrostatic effect, whilst, the hydrodynamic water effect leads the dam to experience severe cracking at the middle zone of the upstream face towards the downstream direction.

Also, **Figure 22** reveals some selected snapshots of the dynamic response of the dam during the analysis to demonstrate the shape deformation of the dam subjected to the seismic motions considering hydrostatic and hydrodynamic pressure effect.

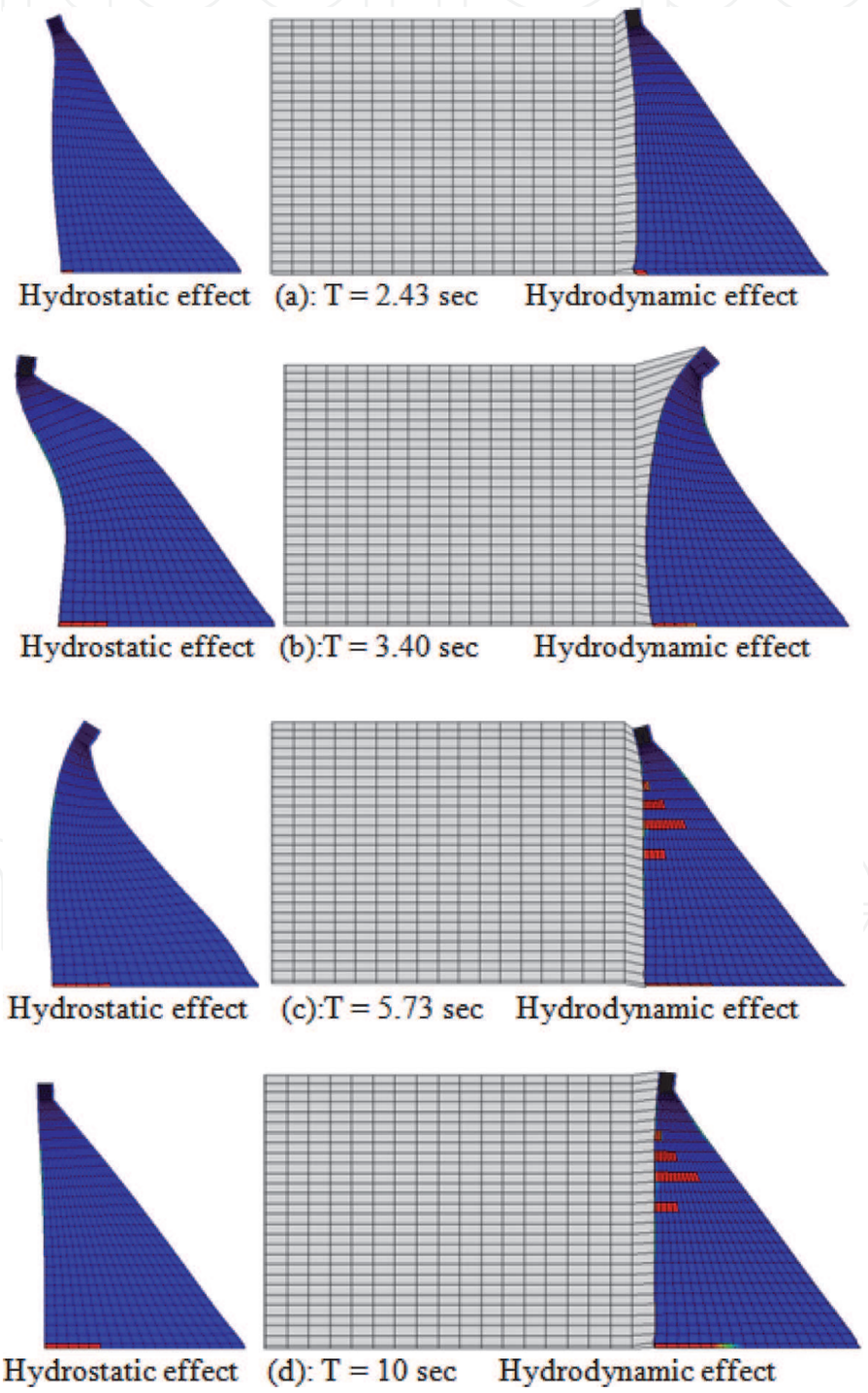

Figure 22.
Snapshots of dam deformation and developed tension cracks in case of both scenarios.

As shown in the figure, different mode shapes at selected times can be observed for the Kinta RCC dam while the hydrostatic and hydrodynamic effect is taken into account. For instance, at the time of 3.40 second and 5.73 second, the mode shapes of the dam is totally dissimilar considering the hydrostatic and hydrodynamic water effect.

7. Conclusions

In this study, an attempt has been made to evaluate the effect of the reservoir hydrostatic and hydrodynamic pressure on the response of RCC dams subjected to earthquake excitations. For this purpose, the Kinta RCC dam has been chosen as a case study and a FEM of the dam-reservoir has been developed. A non-linear seismic analysis of the dam has been conducted in both scenarios. The results of the study have been obtained in terms of acceleration, deformation and displacement, stress and damaged zones. Based on the obtained results, the following conclusions are drawn:

i. The hydrostatic and hydrodynamic pressure exerted at the dam-water interface results higher effects on horizontal than vertical acceleration response.

ii. The nodal displacement of the crest and the heel caused by hydrodynamic effect is increased by 22% in horizontal direction compared to the case when it is omitted. As a result, the relative horizontal displacement of the dam crest is increased by 21% when considering the hydrodynamic pressure effect.

iii. In spite of the fact that, due to considering water weight in hydrodynamic analysis, the nodal displacement of the crest and the heel is decreased by approximately 37% in vertical direction, but the hydrodynamic effect increases the relative vertical displacement of the dam by 67%.

iv. From the maximum and minimum stress analysis, the heel element has the most stress absorption compared to other elements of the dam.

v. Generally, the hydrodynamic effect modifies the deformation shape of the dam during the response and increases the magnitudes of the developed stresses causing more extensive tension crack damages mostly in the heel and upstream zones of the dam.

Eventually, as discussed above, the hydrodynamic pressure highly affects the seismic response and the appearance and extent of the tensile damage zones of the dam. Therefore, for seismic design purposes, this effect has to be seriously taken into consideration.

Author details

Khaled Ghaedi[1,3*], Farzad Hejazi[2], Meisam Gordan[3], Ahad Javanmardi[1,4], Hamed Khatibi[5] and Ali Joharchi[6]

1 Research and Development Center, PASOFAL Engineering, Kuala Lumpur, Malaysia

2 Faculty of Engineering, Housing Research Center, Universiti Putra Malaysia, Malaysia

3 Department of Civil Engineering, University of Malaya, Kuala Lumpur, Malaysia

4 College of Civil Engineering, Fuzhou University, China

5 Faculty of Engineering, Department of Civil and Environmental Engineering, University of Auckland, New Zealand

6 Department of Civil Engineering, Universiti Kebangsaan Malaysia, Selangor, Malaysia

*Address all correspondence to: khaledqhaedi@yahoo.com

References

[1] K. Ghaedi and Z. Ibrahim, "Earthquake Prediction," in *Earthquakes - Tectonics, Hazard and Risk Mitigation*, T. Zouaghi, Ed. InTechOpen, 2017, pp. 205–227.

[2] K. Ghaedi, Z. Ibrahim, H. Adeli, and A. Javanmardi, "Invited Review: Recent developments in vibration control of building and bridge structures," J. Vibroengineering, vol. 19, no. 5, pp. 3564–3580, Aug. 2017.

[3] A. Javanmardi, Z. Ibrahim, K. Ghaedi, M. Jameel, H. Khatibi, and M. Suhatril, "Seismic response characteristics of a base isolated cable-stayed bridge under moderate and strong ground motions," Arch. Civ. Mech. Eng., vol. 17, no. 2, pp. 419–432, 2017.

[4] M. Gordan, H. A. Razak, Z. Ismail, and K. Ghaedi, "Recent developments in damage identification of structures using data mining," Lat. Am. J. Solids Struct., vol. 14, no. 13, pp. 2373–2401, 2017.

[5] A. Javanmardi, Z. Ibrahim, K. Ghaedi, N. B. Khan, and H. Benisi Ghadim, "Seismic isolation retrofitting solution for an existing steel cable-stayed bridge," *PLoS One*, vol. 13, no. 7, p. e0200482, Jul. 2018.

[6] M. U. Hanif, Z. Ibrahim, K. Ghaedi, H. Hashim, and A. Javanmardi, "Damage assessment of reinforced concrete structures using a model-based nonlinear approach – A comprehensive review," Constr. Build. Mater., vol. 192, pp. 846–865, Dec. 2018.

[7] A. Javanmardi, Z. Ibrahim, K. Ghaedi, H. Benisi Ghadim, and M. U. Hanif, "State-of-the-Art Review of Metallic Dampers: Testing, Development and Implementation," Arch. Comput. Methods Eng., vol. 27, no. 2, pp. 455–478, Apr. 2020.

[8] K. Ghaedi, Z. Ibrahim, A. Javanmardi, and R. Rupakhety, "Experimental Study of a New Bar Damper Device for Vibration Control of Structures Subjected to Earthquake Loads," J. Earthq. Eng., pp. 1–19, Sep. 2018.

[9] M. Gordan, H. Abdul Razaka, Z. Ismail, K. Ghaedi, Z. Tan, and H. Ghayeb, "A hybrid ANN-based imperial competitive algorithm methodology for structural damage identification of slab-on-girder bridge using data mining," Appl. Soft Comput., vol. 88, no. 106013, pp. 56–79, 2020.

[10] Y. Calayir and M. Karaton, "Seismic fracture analysis of concrete gravity dams including dam–reservoir interaction," Comput. Struct., vol. 83, no. 19–20, pp. 1595–1606, Jul. 2005.

[11] W. Guanglun, O. A. Pekau, Z. Chuhan, and W. Shaomin, "Seismic fracture analysis of concrete gravity dams based on nonlinear fracture mechanics," Eng. Fract. Mech., vol. 65, pp. 67–87, 2000.

[12] O. Omidi, S. Valliappan, and V. Lotfi, "Seismic cracking of concrete gravity dams by plastic–damage model using different damping mechanisms," Finite Elem. Anal. Des., vol. 63, pp. 80–97, Jan. 2013.

[13] Z. Shi, M. Nakano, Y. Nakamura, and C. Liu, "Discrete crack analysis of concrete gravity dams based on the known inertia force field of linear response analysis," Eng. Fract. Mech., vol. 115, pp. 122–136, 2014.

[14] G. Wang, Y. Wang, W. Lu, C. Zhou, M. Chen, and P. Yan, "XFEM based seismic potential failure mode analysis of concrete gravity dam–water–foundation systems through incremental dynamic analysis," Eng. Struct., vol. 98, pp. 81–94, 2015.

[15] Q. Xu, J. Y. Chen, J. Li, C. B. Zhang, and C. F. Zhao, "The dynamic

characteristics of the damage probability of a gravity dam," J. Appl. Math. Mech., vol. 79, no. 1, pp. 64–70, 2015.

[16] G. Fenves and A. K. Chopra, "Simplified Earthquake Analysis of Concrete Gravity Dams: Separate Hydrodynamic and Foundation Interaction Effects," J. Eng. Mech., vol. 111, no. 6, pp. 715–735, Jun. 1985.

[17] Malkar. P.F, "Nonlinear response of concrete gravity dams to strong earthquake include ground motion," *Comput. Struct.*, vol. 26(1/2), pp. 165–179, 1987.

[18] M. L. Ayari, "A fracture mechanics based seismic analysis of concrete gravity dams using discrete cracks," *Eng. Fract. Mech.*, vol. 35, no. 1/2/3, pp. 587–598, 1990.

[19] R. Espandar and V. Lotfi, "Comparison of non-orthogonal smeared crack and plasticity models for dynamic analysis of concrete arch dams," Comput. Struct., vol. 81, no. 14, pp. 1461–1474, Jun. 2003.

[20] V. Lotfi and R. Espandar, "Seismic analysis of concrete arch dams by combined discrete crack and non-orthogonal smeared crack technique," Eng. Struct., vol. 26, no. 1, pp. 27–37, Jan. 2004.

[21] M. Akkose, A. Bayraktar, and A. a. Dumanoglu, "Reservoir water level effects on nonlinear dynamic response of arch dams," J. Fluids Struct., vol. 24, no. 3, pp. 418–435, Apr. 2008.

[22] M. Akköse and E. Şimşek, "Non-linear seismic response of concrete gravity dams to near-fault ground motions including dam-water-sediment-foundation interaction," Appl. Math. Model., vol. 34, no. 11, pp. 3685–3700, Nov. 2010.

[23] M. E. Kartal, "Three-dimensional earthquake analysis of roller-compacted concrete dams," Nat. Hazards Earth Syst. Sci., vol. 12, no. 2007, pp. 2369–2388, 2012.

[24] S. Zhang, G. Wang, and W. Sa, "Damage evaluation of concrete gravity dams under mainshock–aftershock seismic sequences," Soil Dyn. Earthq. Eng., vol. 50, pp. 16–27, Jul. 2013.

[25] K. Ghaedi, F. Hejazi, Z. Ibrahim, and P. Khanzaei, "Flexible Foundation Effect on Seismic Analysis of Roller Compacted Concrete (RCC) Dams Using Finite Element Method," KSCE J. Civ. Eng., vol. 22, no. 4, pp. 1275–1287, Apr. 2018.

[26] G. Wang, S. Zhang, C. Zhou, and W. Lu, "Correlation between strong motion durations and damage measures of concrete gravity dams," Soil Dyn. Earthq. Eng., vol. 69, pp. 148–162, 2015.

[27] K. Ghaedi, M. Jameel, Z. Ibrahim, and P. Khanzaei, "Seismic analysis of Roller Compacted Concrete (RCC) dams considering effect of sizes and shapes of galleries," KSCE J. Civ. Eng., vol. 20, no. 1, pp. 261–272, Jan. 2016.

[28] Y. Wang and J. Jia, "Experimental study on the influence of hydraulic fracturing on high concrete gravity dams," Eng. Struct., vol. 132, pp. 508–517, Feb. 2017.

[29] J. Wang, G. Yang, H. Liu, S. Shrawan Nimbalkar, X. Tang, and Y. Xiao, "Seismic response of concrete-rockfill combination dam using large-scale shaking table tests," Soil Dyn. Earthq. Eng., vol. 99, pp. 9–19, Aug. 2017.

[30] "Buletin Ingenieur," *Board of Engineers Malaysia*, vol. 29, no. May 2006, pp. 1–57, 2006.

[31] A. M. Huda, M. S. Jaafar, J. Noorzaei, W. A. Thanoon, and T. A. Mohammed, "Modelling the Effects of Sediment on the Seismic Behaviour of

Kinta Roller Compacted Concrete Dam," Pertanika J. Sci. Technol, vol. 18, no. 1, pp. 43–59, 2010.

[32] GHD, "Study of restrictions on RCC temperature, Stage 2 development of Ipoh water supply," 2002.

[33] US Army Corps of Engineers, *Roller-Compacted Concrete*, no. January 2000. 2000.

[34] A. K. Chopra, *Dynamics of Structures Theory and Applications to Earthquake Engineering*, 4th ed. New Jersey: Prentice-Hall, 2012.

[35] M. U. Hanif, Z. Ibrahim, K. Ghaedi, A. Javanmardi, and S. K. Rehman, "Finite Element Simulation of Damage In RC Beams," J. Civ. Eng. Sci. Technol., vol. 9, no. 1, pp. 50–57, 2018.

[36] S. Zhang and G. Wang, "Effects of near-fault and far-fault ground motions on nonlinear dynamic response and seismic damage of concrete gravity dams," Soil Dyn. Earthq. Eng., vol. 53, pp. 217–229, Oct. 2013.

[37] M. U. Hanif, Z. Ibrahim, M. Jameel, K. Ghaedi, and M. Aslam, "A new approach to estimate damage in concrete beams using non-linearity," Constr. Build. Mater., vol. 124, no. C, pp. 1081–1089, 2016.

[38] K. Ghaedi *et al.*, "Finite Element Analysis of A Strengthened Beam Deliberating Elastically Isotropic And Orthotropic Cfrp Material," *J. Civ. Eng. Sci. Technol.*, vol. 9, no. 2, p. 5, Oct. 2018.

[39] J. Lubliner, J. Oliver, S. Oller, and E. Oñate, "A plastic-damage model for concrete," Int. J. Solids Struct., vol. 25, no. 3, pp. 299–326, 1989.

[40] L. J and F. GL, "Plastic-damage model for cyclic loading of concrete structures," J. Eng. Mech., vol. 124, no. 8, pp. 892–900, 1998.

[41] P. N. Patel, C. C. Spyrakos, and W. Virginia, "Uplifting-sliding response of flexible structures to seismic loads," Eng. Anal. Bound. Elem., vol. 8, no. 4, pp. 185–191, 1991.

[42] M. Ftima and P. Léger, "Seismic stability of cracked concrete dams using rigid block models," Comput. Struct., vol. 84, no. 28, pp. 1802–1814, Nov. 2006.

[43] X. Zhu and O. a. Pekau, "Seismic behavior of concrete gravity dams with penetrated cracks and equivalent impact damping," Eng. Struct., vol. 29, no. 3, pp. 336–345, Mar. 2007.

[44] M. Paggi, G. Ferro, and F. Braga, "A multiscale approach for the seismic analysis of concrete gravity dams," Comput. Struct., vol. 122, pp. 230–238, Jun. 2013.

[45] H. Wang, L. Wang, Y. Song, and J. Wang, "Influence of free water on dynamic behavior of dam concrete under biaxial compression," Constr. Build. Mater., vol. 112, pp. 222–231, 2016.